Computational Materials Science 110 (2015) 261–269

Contents lists available at ScienceDirect

Computational Materials Science

journal homepage: www.elsevier.com/locate/commatsci

Effect of Re and W upon brittle fracture in Ni_3Al cracks by atomic simulation

Shu-Lan Liu [a], Chong-Yu Wang [a,b,*], Tao Yu [a]

[a] Central Iron and Steel Research Institute, Beijing 100081, China
[b] Department of Physics, Tsinghua University, Beijing 100084, China

ARTICLE INFO

Article history:
Received 29 April 2015
Received in revised form 13 August 2015
Accepted 15 August 2015
Available online 5 September 2015

Keywords:
Re
W
Brittle fracture
Ni_3Al crack
Molecular dynamics

ABSTRACT

Based on molecular dynamics using the embedded-atom-method potentials and the discrete-variational method for the Ni–Al–Re and Ni–Al–W systems, the effect of Re and W upon the brittle fracture in Ni_3Al cracks at three crack orientations is investigated. The results show that Re and W may strengthen the Ni_3Al alloy and improve the deformation resistance of the materials. The lattice trapping limits are not changed with the addition of a single Re or W atom, but they increase with the addition of 1 and 2 at. % Re or W atoms, and more so with the addition of W atoms. The study reveals that Re and W can prevent bond breaking at the crack tip and can promote crack healing in Ni_3Al, with W exhibiting a stronger effect than Re. Furthermore, the increasing fracture stress values with the increasing concentrations of doping atoms implies that Re and W can improve the brittle fracture strength in Ni_3Al cracks, where W has a stronger effect. These results can be related to the stronger bonding strengths of Ni–Re and Ni–W than that of Ni–Al.

1. Introduction

The intermetallic compound Ni_3Al is an the important strengthening phase for Ni-based superalloys, and has a direct influence upon the mechanical properties of the superalloys for the high corrosion resistance and high strength needed in the aerospace industry [1,2]. In the past few years, the mechanical properties of Ni_3Al have been studied extensively via experiments and theoretical modeling [3–7]. However, the brittle fracture of the Ni_3Al alloy may restrict the application of superalloys as structural materials [1,8].

The final rupture of a material usually results from cracks, and can be understood as the atomic bond breaking at the crack tip, where the fracture manifests discretely with the lattice rather than in a homogeneous continuum from an atomic point of view. The critical fracture stress for a brittle crack to advance is closely related to lattice trapping of the crack first described by Thomson et al. [9]. Owing to the lattice trapping, the discrete atom bonding causes a crack to remain stable (i.e., to not advance or heal) within a certain loading range until the load becomes somewhat larger or smaller than the Griffith load (K^G_{th}). The critical loads for a crack to advance or to heal are respectively called the upper and lower lattice trapping limits ($K^{\pm}_{IC}$). The Griffith load, at which the change in the system total energy is zero when the crack extends in a direction by a certain atomic spacing, with the in-plane borders of the simulation cell fixed [10]. At the Griffith load, a finite lattice-resistance barrier exists between the isoenergetic states, which could trap the crack tip at either state, manifesting the lattice trapping effect [11]. Further studies [11,12] have shown that the lattice trapping strength and range rely upon the interaction range of the interatomic force fields and the relative stiffness of the crack-tip bond. In addition, the directions of the crack front and crack propagation, as well as the interatomic potential, can affect the lattice trapping [13–15]. Generally, the lattice trapping limits are closely related to the fracture stress required for a crack to advance, so to explore the brittle fracture in a Ni_3Al crack it is necessary to study the lattice trapping effect present in the crack.

Rhenium and W are important alloying elements of superalloys [16,17] and have been reported as improving the mechanical properties of Ni_3Al in studies using first-principles calculations [18–20]. Yang and Liu [21,22] studied the effect of Re on Ni_3Al at the atomic scale, and it was found that the bulk modulus of Ni_3Al can be effectively improved by Re and the lattice trapping limits in Ni_3Al crack increased with the addition of some Re atoms. W was found to be beneficial in reducing the coarsening rate of γ' precipitates [23]. It is known that the fracture and strength mechanisms of Ni_3Al are complex, and the previous studies are not sufficient to fully

* Corresponding author at: Department of Physics, Tsinghua University, Beijing 100084, China. Tel.: +86 01062772782.
E-mail addresses: shulan070@126.com (S.-L. Liu), cywang@mail.tsinghua.edu.cn (C.-Y. Wang), ytao012345@163.com (T. Yu).

http://dx.doi.org/10.1016/j.commatsci.2015.08.037
0927-0256/

Table 1
Sample dimensions and the number of atoms (Ni, Al and X, where X stands for Re or W) for the three types of crack systems at the (010)[001], (101)[010] and (010)[101] crack orientations. Each type of Ni_3Al crack system includes three different Re or W concentrations of 0, 1 and 2 at.%.

Crack orientation	System	Dimensions (Å^3)	Number of atoms (Ni + Al + X)
(010)[001]	No	142.68 × 178.35 × 285.36	480,000 + 160,000 + 0
	1 at.% Re	142.73 × 178.41 × 285.46	480,000 + 153,600 + 6400
	1 at.% W	142.77 × 178.46 × 285.54	
	2 at.% Re	142.78 × 178.48 × 285.57	480,000 + 147,200 + 12,800
	2 at.% W	142.85 × 178.56 × 285.70	
(101)[010]	No	151.33 × 151.33 × 285.36	432,000 + 144,000 + 0
	1 at.% Re	151.39 × 151.39 × 285.46	432,000 + 138,240 + 5760
	1 at.% W	151.43 × 151.43 × 285.54	
	2 at.% Re	151.46 × 151.46 × 285.57	432,000 + 132,480 + 11,520
	2 at.% W	151.51 × 151.51 × 285.70	
(010)[101]	No	151.33 × 142.68 × 302.67	432,000 + 144,000 + 0
	1 at.% Re	151.39 × 142.73 × 302.77	432,000 + 138,240 + 5760
	1 at.% W	151.43 × 142.77 × 302.86	
	2 at.% Re	151.45 × 142.78 × 302.89	432,000 + 132,480 + 11,520
	2 at.% W	151.51 × 142.85 × 303.03	

Note: "No" represents the Ni_3Al crack system without doping atoms.

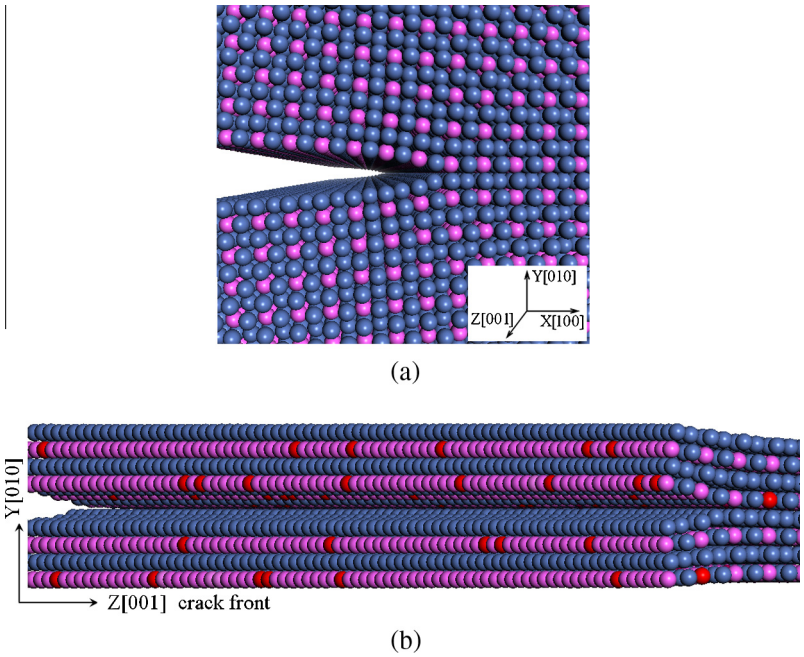

Fig. 1. Atomic configurations of the (010)[001] crack tip at the load of $K_I/K_{th}^G = 1.000$ before relaxation for (a) pure Ni_3Al and (b) Ni_3Al with 2 at.% X (where X = Re, W) atoms. The balls represent the Ni (blue), Al (pink) and X (red) atoms. (For interpretation of the references to colour in this figure legend, the reader is referred to the web version of this article.)

understand the strengthening mechanism of Re and W on Ni_3Al. Therefore, it is essential to explore the influence of Re and W upon fracture in a Ni_3Al crack at the atomic level.

In the present study, Re or W atoms are randomly distributed in Ni_3Al at an atomic ratio of 1 and 2 at.% at the (010)[001], (101)[010] and (010)[101] crack orientations, and the mechanical parameters of Ni_3Al without a crack, the lattice trapping, and the critical fracture stress in a Ni_3Al crack are discussed. Meanwhile, the interatomic energy is calculated using the discrete-variational method (DVM) [24,25] to analyze the effect of Re and W upon the brittle fracture in a Ni_3Al crack.

2. Materials and methods

2.1. Crack model conditions

In the present study, the crack was constructed according to the anisotropic linear elastic continuum mechanics equations [26] with a desired stress intensity factor K_I. Three types of mode I cracks were simulated, which included the (010)[001], (101)[010] and (010)[101] crack orientations. Here, (010) and (101) indicate the directions of the crack planes, and [001], [010] and [101] indicate the directions of the crack front. Fig. 1 shows the atomic configurations of the (010)[001] crack tip for the pure Ni_3Al (Fig. 1(a)) and for the Ni_3Al with 2 at.% X (where X = Re, W) atoms (Fig. 1(b)). The original crack length was set at about l_0 = 45 Å. A periodic boundary condition was used in the direction parallel to the crack front, while fixed-displacement boundary conditions (outermost four atomic layers fixed) were applied in the directions of the crack plane and crack propagation, and the dimensions of these crack systems are listed in Table 1. Furthermore, the calculations were tested with a larger box for each crack orientation, in which the dimension in the z direction was twice that in Table 1. Table 2 lists the values of the elastic constants (C_{ij}), the surface energy (γ), the lattice constant (a) and the upper lattice trapping limit (K_{IC}^+) for the systems with the addition of 0,

Table 2
Values of the elastic constants (C_{ij}), surface energy (γ), lattice constant (a) and upper lattice trapping limits (K_{IC}^{+}) for the systems with the addition of 0, 1 and 2 at.% Re atoms at the (010)[001] crack orientation.

System	Dimensions (atomic layers)	C_{11} (GPa)	C_{12} (GPa)	C_{44} (GPa)	a (Å)	γ (J/m^2)	$\frac{K_{IC}^{+}}{K_{th}^{G}}$
Ni_3Al	80–100–160	242.6	149.3	130.3	3.5671	1.795	1.010
	80–100–320	242.6	149.3	130.2	3.5670	1.795	1.010
Ni_3Al–1 at.% Re	80–100–160	250.5	151.1	131.4	3.5682	1.796	1.020
	80–100–320	250.3	151.2	131.4	3.5681	1.796	1.020
Ni_3Al–2 at.% Re	80–100–160	257.7	152.9	132.4	3.5696	1.798	1.025
	80–100–320	257.8	152.8	132.4	3.5697	1.798	1.025

Note: K_{th}^{G} is the theoretical Griffith stress intensity factor.

Table 3
Average binding energy (E_{eatom}) for the perfect (no crack) Ni_3Al system without dopants and that with Re or W atoms at the (010)[001] crack orientation. The Re–Ni (W–Ni) and Re–Al (W–Al) notations indicate that Re (W) atom substitutes for Ni and Al in Ni_3Al, respectively.

System	E_{eatom} (eV/atom)
Ni_3Al	
Previous[a]	−4.63
This work	−4.65
Ni_3Al–Re	
1 at.% Re	
Re–Ni	−4.68
Re–Al	−4.69
2 at.% Re	
Re–Ni	−4.71
Re–Al	−4.73
Ni_3Al–W	
1 at.% W	
W–Ni	−4.68
W–Al	−4.69
2 at.% W	
W–Ni	−4.70
W–Al	−4.74

[a] [37].

1 and 2 at.% Re atoms at the (010)[001] crack orientation, and it was found that these calculation results were insensitive to the change of the simulation size. Therefore, the smaller boxes described in Table 1 were chosen for the simulations in the present study. The system temperature remained at a constant value of 300 K, which was obtained by scaling the instantaneous velocities of all atoms with the appropriate Maxwell–Boltzmann distribution. In the molecular dynamics (MD) simulation, Newton's equations of motion were calculated using the Gear Algorithm [27], and the time step was 5×10^{-15} s. The embedded-atom-method (EAM) potentials of Ni–Al–Re and Ni–Al–W were applied [28,29], and can successfully describe the Ni–Al–X (where X = Re, W) crack systems [21,30,31]. Finally, the XMD program [32] was used in the present study.

To test the site preference behavior of Re and W in Ni_3Al, the average binding energy (E_{eatom}) of the perfect system at the (010)[001] crack orientation was calculated using the MD method. The average binding energy is defined as

$$E_{eatom} = \frac{E_{total}}{N}, \tag{1}$$

where E_{total} is the total energy of the perfect system and N is the total number of atoms for the entire system; E_{eatom} is the ratio of E_{total} and N, and it is the average energy of every atom for the system. Table 3 lists the calculation results for the systems with 0, 1 and 2 at.% Re (or W) atoms randomly doped to the Ni or Al sites. Lower values of E_{eatom} indicate a more stable system and predicate that Re or W atom prefers to occupy the corresponding site, so it can be concluded from Table 3 that Re and W atoms will preferentially occupy the Al sites, which is in agreement with the experimental and theoretical results [33–36]. In the present study, therefore, Re and W atoms were substituted for Al sites in all of the doped systems. In addition, for pure Ni_3Al, the difference between the E_{eatom} values of the present result (−4.65 eV) and the previous result (−4.63 eV) [37] is negligible.

2.2. Simulation method

In the lattice trapping simulations, the cracks were initially configured at different loads, and were subsequently fully relaxed with the above boundary conditions. The loading or unloading was initiated at a stress intensity that fulfilled the Griffith criterion, wherein the crack tip is stable and does not advance or heal. The relaxed configurations were then taken as the starting structures for further loading or unloading by proportional scaling of the boundary displacements, where the increment of loading or unloading was 0.5% of the Griffith load (K_{th}^{G}). Finally, the upper and lower trapping limits ($K_{IC}^{\pm}$) were determined by the sudden increase and decrease of the average bond lengths, respectively, along the crack front of the crack tip (Fig. 2). Accordingly, the lattice trapping range (ΔK) was determined as [15,30]

$$\Delta K = K_{IC}^{+}/K_{IC}^{-} - 1. \tag{2}$$

After thus obtaining the upper lattice trapping limit (K_{IC}^{+}), the fracture stress (σ_{IC}^{+}) for the crack to advance was estimated using [24,30]

$$\sigma_{IC}^{+} \approx K_{IC}^{+}/\sqrt{l}, \tag{3}$$

where l is the crack length.

3. Results and discussion

3.1. Effect of Re and W upon mechanical parameters

To estimate the reliability of the EAM potentials of Ni–Al–Re and Ni–Al–W, we calculate the three independent elastic constants (C_{11}, C_{12}, C_{44}), the bulk modulus (B), the shear modulus (G), Young's modulus (E) and the lattice constant (a) beforehand for the perfect (no crack) Ni_3Al with 0, 1 and 2 at.% Re (or W) atom doping. Herein the bulk modulus (B) is obtained by $B = (C_{11} + 2C_{12})/3$, and the shear modulus (G) is calculated as the arithmetic Hill average [38] $G = (G_V + G_R)/2$, where $G_V = (C_{11} - C_{12} + 3C_{44})/5$ and $G_R = 5/(4S_{11} - 4S_{12} + 3S_{44})$ (S_{11}, S_{12} and S_{44} are the elastic compliances

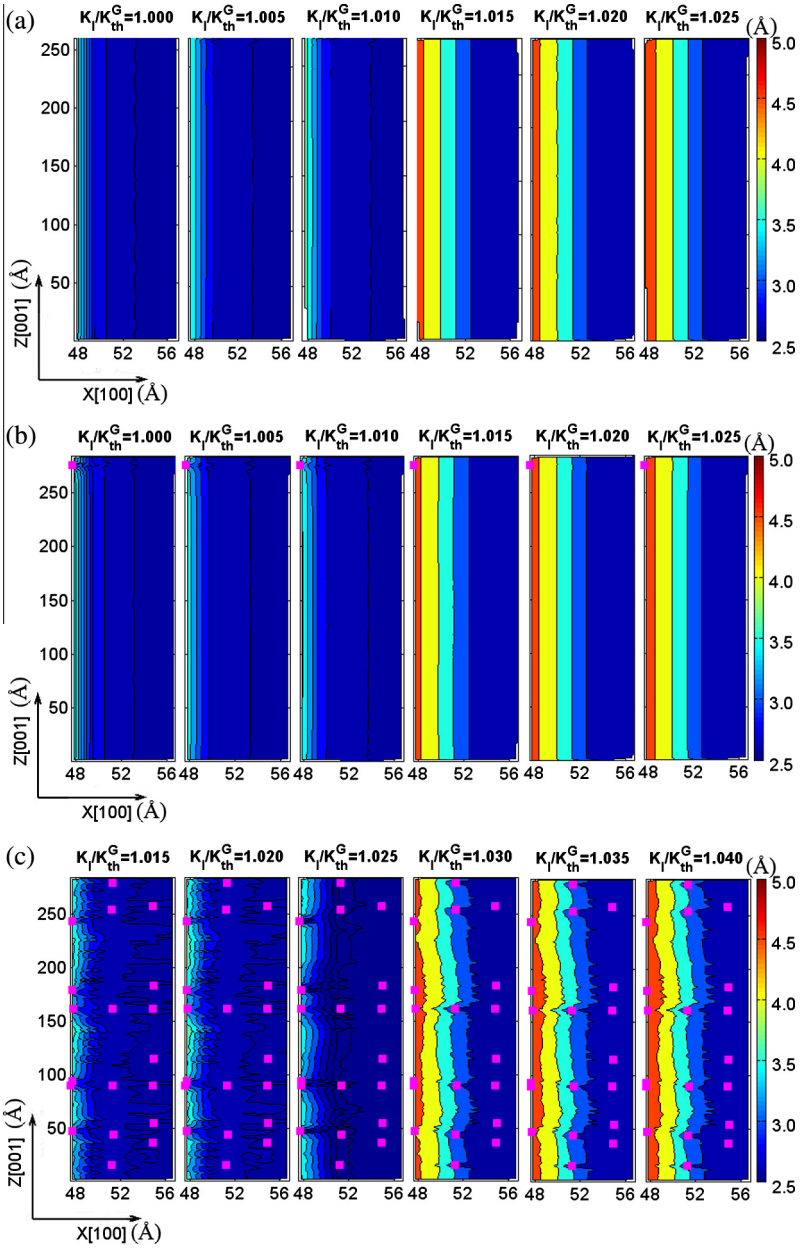

Fig. 2. Contour maps of atom pair bond lengths at the crack tip across the (0 1 0)[0 0 1] crack surface during the loading process for (a) pure Ni_3Al, (b) Ni_3Al with the addition of a single Re atom, and (c) Ni_3Al with the addition of 2 at.% Re atoms. The pink squares represent the positions of the Re atoms, and bond lengths are represented by the color spectrum defined by the bar legends on the right. (For interpretation of the references to colour in this figure legend, the reader is referred to the web version of this article.)

[39]) are the Voigt and Reuss bounds, respectively. Young's modulus (E) is then obtained as $E = 9\,GB/(G + 3B)$.

Table 4 lists the calculation results of the mechanical parameters for the perfect Ni_3Al with and without the addition of 1 and 2 at.% Re (or W) atoms. It can be found from Table 4 that the values of B, G and E all increase with the addition of Re or W atoms, which is consistent with previous studies [40,41]. In addition, for higher concentrations of Re or W atoms, the values of B, G and E are seen to increase, which indicates that Re and W may strengthen the Ni_3Al alloy and improve the deformation resistance of the material. Furthermore, the lattice constants of the systems increase with the addition of Re or W atoms, which is consisted with the previous study [41], and the variation of lattice constant may be related with the large atomic radii of alloying elements (Re and W) and the interatomic interaction. Finally, for the pure Ni_3Al, the difference between the C_{ij} value of the present study and that of the previous theoretical and experimental results [37,42,43] is negligible. From the above results, it can be seen that the potentials of Ni–Al–Re and Ni–Al–W can well describe the systems in the present study.

3.2. Effect of Re and W upon lattice trapping of the crack

In this section, two doping configurations are considered, wherein the first is a single Re (or W) atom placed at the crack tip to investigate the lattice trapping effect in a single-impurity model; and the other is the random distribution of 1 and 2 at.% Re (or W) atoms in the system to explore the effect of increasing Re or W atomic concentrations upon the lattice trapping in the Ni_3Al crack.

Table 4
Mechanical parameters of the Ni_3Al with (1 and 2 at.%) and without Re or W atoms, including the elastic constants (C_{11}, C_{12}, C_{44}), bulk modulus (B), shear modulus (G), Young's modulus (E) and lattice constant (a).

System	C_{11} (GPa)	C_{12} (GPa)	C_{44} (GPa)	B (GPa)	G (GPa)	E (GPa)	a (Å)
Ni_3Al							
This work	242.6	149.3	130.3	180.4	86.4	223	3.5670
EAM[a]	236	154	127				3.571
F-P[b]	242.2	151.8	125.4				3.57
Exp[c]	230.0	150.0	131.0				3.57
Ni_3Al–Re							
1 at.% Re	250.5	151.1	131.4	184.2	89.0	230	3.5682
2 at.% Re	257.8	152.8	132.4	187.8	91.4	236	3.5696
Ni_3Al–W							
1 at.% W	244.2	151.5	131.2	182.4	86.5	224	3.5692
2 at.% W	249.8	153.1	132.1	185.3	88.3	229	3.5712

[a] [37].
[b] [42].
[c] [43].

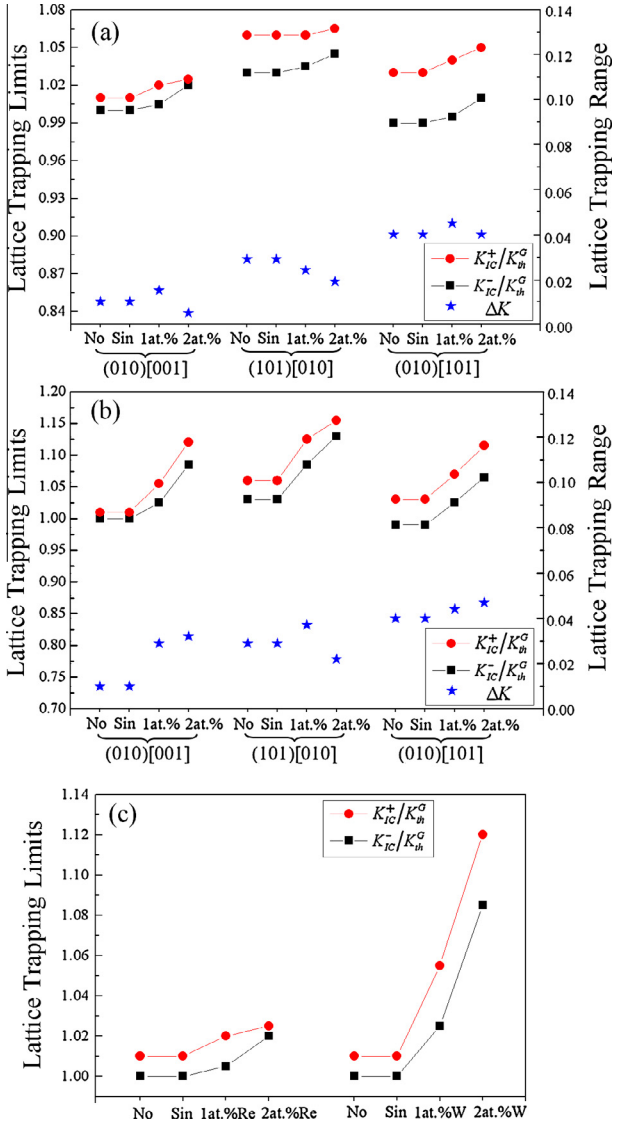

Fig. 3. (a–b) Lattice trapping limits and trapping ranges at the (010)[001], (101)[010] and (010)[101] crack orientations in Ni_3Al without doping (No), with a single doping atom (Sin), and with 1 and 2 at.% doping atoms of (a) Re and (b) W. (c) Lattice trapping limits for Ni_3Al with and without Re or W at the (010)[001] crack orientation.

3.2.1. Influence of a single Re or W atom upon lattice trapping of the crack

To calculate the lattice trapping limits and range, a single Re or W atom is placed at the crack tip at each crack orientation, where the variations of the bond lengths along the (010)[001] crack front with the loading stress intensity factor are shown in Fig. 2(b). From the relationship of the bond length to K_I/K_{th}^{G} in Fig. 2(a), we find that there are slight jumps in the bond lengths between the values $K_I/K_{th}^{G} = 1.010$ and 1.015, and the bond lengths clearly increase when $K_I/K_{th}^{G} > 1.010$. Therefore, it can be determined that the upper lattice trapping limit for Ni_3Al without doping atom at the (010)[001] crack orientation is $K_{IC}^{+} = 1.010K_{th}^{G}$. It can be found by comparing Fig. 2(a) and (b) that, for the system with a single Re atom and that with a single W atom, the jumps of bond lengths at the crack tip occur between $K_I/K_{th}^{G} = 1.010$ and 1.015, which means that a single Re or W atom has no influence upon K_{IC}^{+} at the (010)[001] crack tip. With the same method and by observing the sudden decrease of bond lengths at the crack tip, we can obtain the lower lattice trapping limit for the system with a single Re or W atom ($K_{IC}^{-} = 1.000K_{th}^{G}$), and find likewise that a single Re or W atom has no effect upon K_{IC}^{-} at the (010)[001] crack tip.

Fig. 3(a) and (b) show the lattice trapping limits ($K_{IC}^{\pm}$) and trapping ranges (ΔK) for systems with a single Re or W atom at the three crack orientations ((010)[001], (101)[010] and (010)[101]), where we can observe that the values of $K_{IC}^{\pm}$ and ΔK are not changed with the addition of a single Re or W atom. This implies that a single Re or W atom does not affect the lattice trapping limits and trapping range in a single-impurity model. Models with the other three different positions of a single Re or W atom along the crack front were also simulated, and it can be likewise seen that the lattice trapping limits and trapping ranges are not influenced by the different positions of a single Re or W atom at the crack tip.

Furthermore, it is noticed that the bond breaking (or healing) of several consecutive atomic rows at the crack tip takes place simultaneously, which can be observed in Fig. 2(a) and (b) by the variation in the colors signifying the bond lengths along the direction of the crack propagation. Therefore, the bond breaking or healing in a Ni_3Al crack should be determined based upon the observations of several consecutive atomic rows at the crack tip. At the same time, it can be seen that there is slight bending in the atomic rows near the Re or W atom along the direction perpendicular to the crack propagation during the loading process before the bond breaking

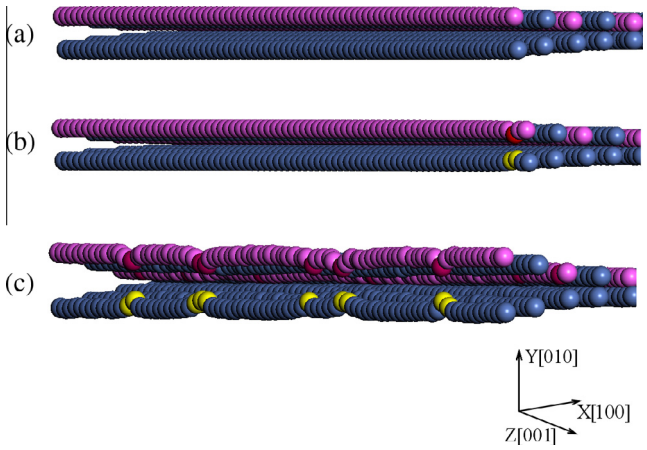

Fig. 4. Atomic configurations of the upper and lower crack surfaces at the (010)[001] crack tip for (a) pure Ni_3Al, (b) Ni_3Al with a single Re atom at the crack tip at the load of $K_I/K^G_{th} = 1.005$, and (c) Ni_3Al with 2 at.% Re atoms at the load of $K_I/K^G_{th} = 1.020$. The blue, pink, red and yellow balls represent Ni, Al, Re and Ni (near Re atoms in the lower crack surface) atoms, respectively. (For interpretation of the references to colour in this figure legend, the reader is referred to the web version of this article.)

Table 5
Lattice trapping limits ($K^{\pm}_{IC}$) with four different doping randomness distributions (A, B, C, D) at the (010)[001] crack orientation for the systems with 2 at.% Re and W atom, respectively.

Randomness distribution	Ni_3Al – 2 at.% Re		Ni_3Al – 2 at.% W	
	$\frac{K^-_{IC}}{K^G_{th}}$	$\frac{K^+_{IC}}{K^G_{th}}$	$\frac{K^-_{IC}}{K^G_{th}}$	$\frac{K^+_{IC}}{K^G_{th}}$
A	1.020	1.025	1.085	1.120
B	1.015	1.025	1.085	1.120
C	1.020	1.025	1.090	1.125
D	1.020	1.025	1.085	1.120

Note: K^G_{th} is the theoretical Griffith stress intensity factor.

(Fig. 2(b) from $K_I/K^G_{th} = 1.000$–1.010 and Fig. 4(b)). This means that the interatomic interaction of Ni–Re and Ni–W may be stronger than that of Ni–Al, which will be discussed in Section 3.4. However, when the loading value of $K_I/K^G_{th} = 1.015$ is reached (Fig. 2(b)), the bond breakings of the Ni–Re and Ni–W are simultaneous with those of the Ni–Al bonds along the crack front. This reveals that the bending of the atomic rows has no influence upon the lattice trapping limits in a single-impurity model.

3.2.2. Influence of Re or W atomic concentrations upon the lattice trapping of the crack

First, to test the influence of different doping randomness upon the lattice trapping and to confirm the reliability of random doping, four different random distributions of 2 at.% Re and W in Ni_3Al are simulated at the (010)[001] crack orientation, respectively, and the values of $K^{\pm}_{IC}$ are listed in Table 5. It can be found from Table 5 that the errors of the $K^{\pm}_{IC}$ values for the four different distributions are negligible, which suggests that the lattice trapping limits are insensitive to the varying of the doping randomness. Thus, random doping is reliable for the present study, and the atomic configuration of the Ni_3Al crack system with 2 at.% Re (or W) atoms at the (010)[001] crack orientation used in this study is given in Fig. 1(b).

As shown in Fig. 3, the lattice trapping limits and ranges for the systems with and without Re or W atoms at each crack orientation are given, and it can be seen that the values of $K^{\pm}_{IC}$ all increase with the addition of 1 and 2 at.% Re (Fig. 3(a)) or W (Fig. 3(b)) atoms. As an example, with the addition of 2 at.% Re atoms, the values of K^+_{IC}/K^G_{th} (K^-_{IC}/K^G_{th}) at the three crack orientations of (010)[001], (101)[010] and (010)[101] are found to be 1.025 (1.020), 1.065 (1.045) and 1.050 (1.010), respectively, and are each increased by a magnitude of 1.5% (2%), 0.5% (1.5%) and 2.0% (2.0%), respectively, over those of the pure Ni_3Al (1.010 (1.000), 1.060 (1.030) and 1.030 (0.990), respectively. As the atomic concentration of Re or W is increased, the values of $K^{\pm}_{IC}$ also increase, which suggests that Re and W can promote crack healing and prevent the advancement of cracks (i.e., the atomic bond breaking at the crack tip). Moreover, it is noticed that the rate of increase of the $K^{\pm}_{IC}$ magnitudes are different for systems with the same atomic concentration of Re or W at the same crack orientation. For example, the values of $K^{\pm}_{IC}$ for the (010)[001] crack system with 1 and 2 at.% W atoms are larger than those with 1 and 2 at.% Re atoms (Fig. 3(c)). The increases in the magnitudes of K^+_{IC} (K^-_{IC}) for the systems with 1 at.% Re and W atoms are 2.5% (0.5%) and 4.5% (0.9%), respectively. This means that different alloying elements have a different degree of influence upon the lattice trapping limits, and the effect of W is seen to be stronger than that of Re. The reason for this difference between the two types of atoms may be related to the different bonding strengths of Ni–Re and Ni–W. However, it can be seen in Fig. 3(a) and (b) that the lattice trapping ranges are all small (the largest is no more than 5%) at the three crack orientations, even though 1 or 2 at.% Re (or W) atoms are doped into the crack system. This may be related to the long-range interatomic potential [21,30]. It has been reported that the lattice trapping of bond breaking at the crack tip is negligible for the long-range interatomic potential [11], so the small trapping range present in this study implies that the interatomic interactions of Ni–Re and Ni–W also has long-range characteristics.

Comparing the values of $K^{\pm}_{IC}$ in Fig. 3(a) and (b), it is obvious that at different crack orientations there are different lattice trapping limits and trapping ranges for the systems with the same Re or W atomic concentration. As an example, the values of the K^-_{IC}/K^G_{th} ratio for the systems without doping atoms at the three crack orientations of (010)[001], (101)[010] and (010)[101] are 1.000, 1.030 and 0.990 (Fig. 3(a) and (b)), respectively; for those with 1 at.% Re the values are 1.005, 1.035 and 0.995 (Fig. 3(a)), respectively; and for those with 1 at.% W the values are 1.025, 1.085 and 1.025 (Fig. 3(b)), respectively. The reason for these differences between the different crack orientations is that the cleavage fracture of the material is directionally anisotropic, and so the degree

Table 6
Values of the $K^+ = K^+_{IC}/K^G_{th}$ ratio, the surface energy (γ), the anisotropic elasticity term ($\delta\beta$) and the fracture stress (σ^+_{IC}) for the Ni_3Al crack systems with (1 and 2 at.%) and without (No) Re or W doping atoms at the (010)[001], (101)[010] and (010)[101] crack orientations.

Crack orientation	System	K^+	γ (J/m^2)	$\delta\beta(\times 10\sqrt{\text{Pa}})$	σ^+_{IC} (GPa)
(010)[001]	No	1.010	1.795	4.654	7.491
	1 at.% Re	1.020	1.796	4.743	7.713
	2 at.% Re	1.025	1.798	4.817	7.875
	1 at.% W	1.055	1.807	4.666	7.871
	2 at.% W	1.120	1.822	4.681	8.364
(101)[010]	No	1.060	1.883	4.654	8.053
	1 at.% Re	1.060	1.886	4.743	8.213
	2 at.% Re	1.065	1.890	4.817	8.389
	1 at.% W	1.125	1.899	4.666	8.604
	2 at.% W	1.155	1.917	4.670	8.884
(010)[101]	No	1.030	1.795	4.871	7.996
	1 at.% Re	1.040	1.796	4.945	8.198
	2 at.% Re	1.050	1.798	5.006	8.383
	1 at.% W	1.070	1.808	4.888	8.366
	2 at.% W	1.115	1.822	4.899	8.770

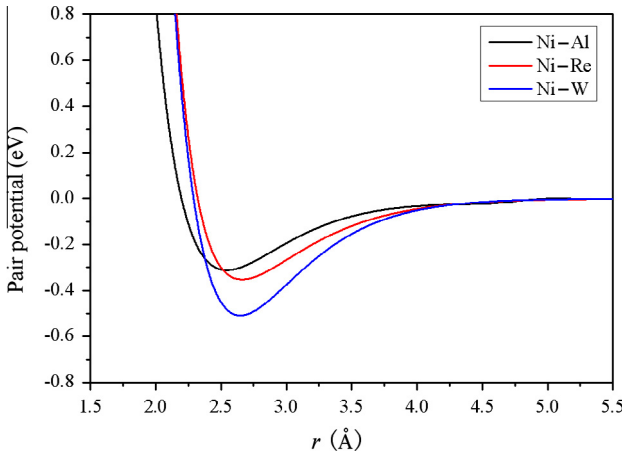

Fig. 5. Variations of the pair potential of Ni–Al, Ni–Re and Ni–W with the atomic distance (r) in the EAM potentials.

of difficulty for the crack to advance is different at different directions of the crack front or crack propagation [14,15,37]. Thus, the loads necessary for a crack to heal or to advance at different crack orientations are different, which indicates that the lattice trapping effect relies upon the directions of the crack front and crack propagation. In addition, for the systems at the (101)[010] crack orientation with or without the addition of Re or W atoms, the values of the K_{IC}^{-}/K_{th}^{G} ratio are greater than 1.000 (the lower lattice trapping limits are greater than K_{th}^{G}), which means that the stability ranges do not include K_{th}^{G}. This may be related to the surface energy (γ), which can be obtained using the relation [21,31]

$$\gamma = (E_{off} - E_{on})/(2S), \tag{4}$$

where E_{off} is the potential energy of the model with a periodic boundary condition in the x and z directions, and a free boundary condition in the y direction; E_{on} is the potential energy of the model with a periodic boundary condition in the x, y and z directions; and S is the area of the y plane. The calculated values of γ at different crack orientations for the present study are listed in Table 6, and it is apparent that the surface energy of the (101) plane is larger than that of the (010) plane for systems with and without the addition of Re or W atoms. As an example, the value of γ for the system without doping atoms is 0.088 J/m^2 larger for the (101) plane compared with the (010) planes, with 1 at.% Re doping atoms it is 0.087 J/m^2 larger, and with 1 at.% W doping atoms it is 0.092 J/m^2 (and 0.091 J/m^2) larger. According to the Griffith theory of brittle fracture, a plane with a lower surface energy should be the preferred cleavage plane, and a crack will prefer to propagate on this plane. Hence, the (101) plane requires a larger load for crack propagation than the (010) plane.

There are no kink pairs or dislocation emissions during the loading or unloading process, for all of the crack systems containing 1 and 2 at.% Re (or W) atoms. However, bending of the atomic rows near the Re (or W) atoms can be seen along the direction perpendicular to the crack propagation along the crack front (Fig. 4(c)), which is also seen with a single Re (or W) atom at the crack tip (Fig. 4(b)). Moreover, the bending of the atomic rows can also be seen by the variation in the colors of the contour maps signifying the bond lengths at the crack tip. As an example, in the contour maps of the atom pair bond lengths for different loads (Fig. 2(c)), the system containing 2 at.% Re atoms at the (010)[001] crack orientation exhibits bending of the atomic rows near the Re atoms (located near the pink squares) along the crack front at about x = 48 Å in the load range $K_I/K_{th}^{G} = 1.015$—1.025 and at about x = 52 Å in the load range $K_I/K_{th}^{G} = 1.030$—1.040. This suggests that there are stronger interactions between the Re (or W) and Ni atoms than between the Al and Ni atoms.

For metal material, it is difficult to study the lattice trapping of cracks directly via experiments because the metal is not brittle enough and does not show large trapping effect [21,30,44]. However, the trend of the effect of Re and W upon the improvement of mechanical properties of Ni_3Al in the present study can be supported by the previous theoretical and experimental results [37,42,43].

3.3. Effect of Re and W upon the fracture stress of the crack

After obtaining the upper lattice trapping limit (K_{IC}^{+}) of a crack, the fracture stress (σ_{IC}^{+}) for the crack to advance can be estimated from Eq. (3). In the present study, we mainly explore the influence of 1 and 2 at.% Re (and W) atoms upon the fracture stress. In the calculation of the fracture stress, the theoretical Griffith stress intensity factor (K_{th}^{G}) can be obtained using [26,30]

$$K_{th}^{G} = (2\gamma/\pi)^{1/2}\left\{(\beta_{11}\beta_{22}/2)^{1/2}[(\beta_{22}/\beta_{11})^{1/2} + (2\beta_{12}+\beta_{66})/2\beta_{11}]^{1/2}\right\}^{-1/2}, \tag{5}$$

where γ is the surface energy of the system (Eq. (4)), and β_{ij} (where i, j = 1, 2, 3, 4, 5, 6) is the plane strain compliance coefficient (more calculation details for the matrix element β_{ij} can be found in the literature [30,45]), wherein we take the second term $\left\{(\beta_{11}\beta_{22}/2)^{1/2}[(\beta_{22}/\beta_{11})^{1/2} + (2\beta_{12}+\beta_{66})/2\beta_{11}]^{1/2}\right\}^{-1/2}$ as the anisotropic elasticity term ($\delta\beta$).

Combining Eq. (3) and the $K^{+} = K_{IC}^{+}/K_{th}^{G}$ ratio (Fig. 3(a) and (b)), the fracture stress can be estimated using $\sigma_{IC}^{+} \approx K_{IC}^{+}/\sqrt{l} = K^{+}\cdot K_{th}^{G}/\sqrt{l}$, and the calculation results for the surface energy (γ), the anisotropic elasticity term ($\delta\beta$) and the fracture stress (σ_{IC}^{+}) for the systems with and without Re or W atoms are tabulated in Table 6. It can be seen from the values of σ_{IC}^{+} that, for all of the crack systems with and without Re or W atoms, the largest fracture stresses are at the (101)[010] crack orientation and the smallest are at the (010)[001] crack orientation. This is because the values of γ and $\delta\beta$ at the (101)[010] crack orientation are the largest of the three crack orientations, and the values of $\delta\beta$ at the (010)[001] crack orientation are the smallest. This implies that the fracture stress for crack propagation mainly relies upon the surface energy and the anisotropic elasticity term. Meanwhile, in the systems with 2 at.% W, it can be seen that the value of K^{+} at the (010)[001] crack orientation (1.120) is larger than that of the (010)[101] crack orientation (1.115), while the value of σ_{IC}^{+} of the former (8.364 GPa) is smaller than that of the latter (8.770 GPa). This means that the fracture stress has a low correlation with the K_{IC}^{+}/K_{th}^{G} ratio, which may be owing to the small lattice trapping range.

Comparing the values of σ_{IC}^{+} in Table 6 for the systems with different atomic concentrations of Re or W, it can be found that higher atomic concentrations correlate with larger fracture stress. On the other hand, the values of σ_{IC}^{+} are different for the systems with the same amount of Re or W atoms at different crack orientations, which means that the atomic concentration of Re or W and the directions of the crack front and crack propagation can all affect the fracture stress of a crack. Furthermore, for the systems with equal dopant concentrations, the values of σ_{IC}^{+} for the systems doped with W atoms are larger than those doped with Re atoms at the three crack orientations. As an example, for the (010)[001] crack system, the fracture stress values are 3.0% and 5.1% larger with 1 and 2 at.% Re atoms, respectively, compared with the

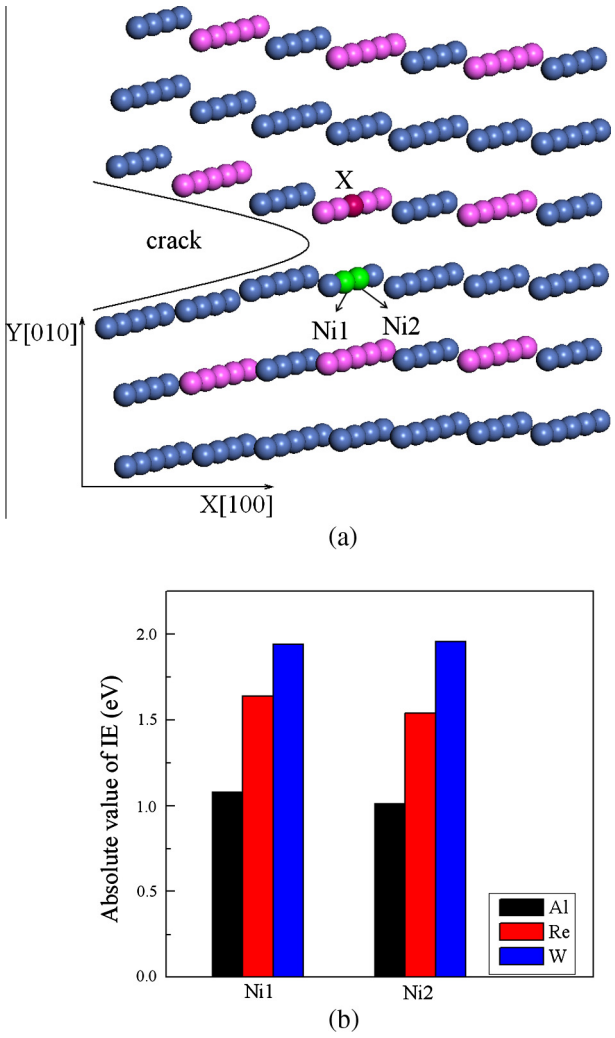

Fig. 6. (a) Atomic configurations of the DVM calculation including 189 atoms. The balls represent the Ni (blue), Al (pink) and *X* (red) (*X* = Al, Re, W) atoms, and the two green balls (Ni1 and Ni2) represent the nearest-neighbor atoms of X. (b) Absolute values of the interatomic energies existing between X and the Ni1 or Ni2 atoms. (For interpretation of the references to colour in this figure legend, the reader is referred to the web version of this article.)

values of the system without doping atoms; and they are 5.1% and 11.7% larger with 1 and 2 at.% W atoms, respectively. This implies that different elements have a different degree of influence upon the brittle fracture in the Ni_3Al crack, where we specifically find that W has a stronger effect than Re.

3.4. Bonding strength between atoms

In the present work, we find that Re and W doping affect the mechanical parameters of Ni_3Al and the lattice trapping limits and fracture stress of the Ni_3Al crack. These properties may be related to the different interatomic interactions between atoms, making it necessary to investigate the bonding strengths of Ni–Re, Ni–W and Ni–Al.

3.4.1. Bonding strengths estimated from the pair potential in the EAM potential

First, the bonding strength between atoms can be roughly estimated from the well depth of the pair potential in the EAM potential [21,30,31,46]. Fig. 5 plots the curves of the well depths of the pair potentials of Ni–Al, Ni–Re and Ni–W with the atomic distance (r) in the EAM potentials, where the curve minima for Ni–Al, Ni–Re and Ni–W are located at r = 2.52, 2.65 and 2.64 Å, respectively, and at the absolute values of the pair potential are 0.31, 0.35 and 0.51 eV, respectively. This confirms that the bonding strengths of Ni–Re and Ni–W are greater than that of Ni–Al, with bonds that are calculated to be 16% (Ni–Re) and 61% (Ni–W) stronger.

3.4.2. Bonding strengths calculated from DVM

It is known that the bonding strength between atoms in a local region can be evaluated by the interatomic energy (IE), which is defined as [47,48]

$$E_{lm} = \sum_{n}\sum_{\alpha\beta} N_n a^{*}_{n\alpha l} a_{n\beta m} H_{\beta m\alpha l}, \tag{6}$$

where N_n is the electron occupation number for molecular orbital ψ_n; $H_{\beta m\alpha l}$ is the Hamiltonian matrix element that connects the atomic orbital β of atom m to the atomic orbital α of atom l; and the coefficient $a_{n\alpha l}$ is obtained from $a_{n\alpha l} = \langle \phi_{\alpha l} | \psi_n(r) \rangle$, with a corresponding relation for the coefficient $a_{n\beta m}$. The IE can be used to evaluate the bonding strength of two adjacent atoms because it is related to the Hamiltonian matrix element and the wave vector matrix in the representation. Generally, a large negative IE value correlates to a strong interatomic interaction. The IE can be obtained using the DVM calculation. The Discrete Variational Method (DVM) [49,50] is an all-numerical self-consistent method based on density functional theory (DFT), in which the one-electron wave-functions of the molecule or the cluster are expanded on a basis of numerical atomic orbitals (NAO), obtained from DFT calculations for atoms or ions. DVM is suitable to treat large molecules and sizable clusters representing solid-state systems. Heavy atoms may also be included, such as transition-metals, lanthanides and actinides. The DVM calculation has been successfully used to describe the electronic structures of metals and alloys [24,25].

The crack model for pure Ni_3Al at the (010)[001] orientation (Table 1) is chosen to perform the IE calculation, whereupon a single Re or W atom is placed at the center of the crack tip along the crack front. First, a model including 640,000 atoms is relaxed using the MD method, after which a cluster of 189 atoms located at the center of the MD model (Fig. 6(a)), is selected to calculate the IE using the DVM. Two Ni atoms (Ni1 and Ni2) are identified as the nearest-neighbor atoms of the atom X, where X is the location of an Al atom or of the dopant atom Re or W, and a calculation of the spin-polarization is carried out. The calculation results of the absolute values of the IE between the X (X = Al, Re, W) and the Ni1 (or Ni2) atoms are shown in Fig. 6(b), where it can be seen that the absolute IE values between the dopant atoms (Re or W) and Ni1 or Ni2 are larger than that of the Al atom. As an example, the absolute IE values of Ni1–Re (1.64 eV) and Ni1–W (1.95 eV) exhibit a 51% and 80% increase over that of Ni1–Al (1.08 eV), respectively. This indicates that the bonding strengths of Ni–Re and Ni–W are stronger than that of Ni–Al, with W exhibiting a stronger effect than Re, which is a result that is consistent with that found in Section 3.4.1.

In summary, because of the greater bonding strengths of Ni–Re and Ni–W compared with that of Ni–Al, Re and W are able to prevent the bond breaking of the crack tip and promote the crack healing in Ni_3Al, thereby improving the mechanical properties and increasing the fracture stress of the Ni_3Al crack. Additionally, W has a stronger effect than Re for improving the brittle fracture in the Ni_3Al crack. The present study may provide useful information and a good theoretical guidance for the design of Ni-based superalloys in the future research.

4. Conclusions

In the present study, the MD simulations and the DVM calculation are used to investigate the effect of Re and W upon the brittle fracture in a Ni_3Al crack at the three crack orientations (0 1 0)[0 0 1], (1 0 1)[0 1 0] and (0 1 0)[1 0 1]. The calculation results are as follows:

(1) The values of B, G and E increase with the addition of 1 and 2 at.% Re (or W) atoms, indicating that Re and W may strengthen the Ni_3Al alloy and improve the deformation resistance of materials.
(2) A single Re or W atom does not influence the lattice trapping limits, but the calculated values of $K_{IC}^{\pm}$ increase with the addition of 1 and 2 at.% Re (or W) atoms, and especially with the addition of W atoms. This indicates that Re and W can prevent crack advancement and promote crack healing in Ni_3Al, with W exhibiting a stronger effect than Re.
(3) The increasing magnitude of $\sigma_{IC}^{\pm}$ with doping concentrations indicate that Re and W can improve the brittle fracture stress of the Ni_3Al crack, with W exhibiting a better effect. Moreover, it is noticed that the fracture stress of a crack is related to the surface energy and the anisotropic elasticity term.
(4) The results of the DVM calculation and the pair potential in the EAM potential indicate that the bonding strengths of Ni–Re and Ni–W are greater than that of Ni–Al, with Ni–W exhibiting the strongest bond.

Acknowledgments

This work was supported by the National Basic Research Program of China (Grant No. 2011CB606402) and the National Natural Science Foundation of China (Grant No. 51071091). The simulations were performed using the "Explorer 100" cluster system at the Tsinghua National Laboratory for Information Science and Technology, Beijing, China.

References

[1] G.X. Yang, Y.F. Xu, L. Jiang, S.H. Liang, Prog. Nat. Sci.: Mater. Int. 21 (2011) 418–425.
[2] H. Yu, Y. Su, N. Tian, S. Tian, Mater. Sci. Eng., A 565 (2013) 292–300.
[3] A. Korner, Philos. Mag. A 63 (1991) 407–421.
[4] N. Baluc, R. Schäublin, Philos. Mag. A 74 (1996) 113–136.
[5] H.X. Xie, B. Liu, T. Yu, Philos. Mag. 92 (2012) 1542–1553.
[6] H.X. Xie, T. Yu, F. Yin, C.C. Tang, Mater. Sci. Eng., A 580 (2013) 99–104.
[7] A.H.W. Ngan, M. Wen, C.H. Woo, Comput. Mater. Sci. 29 (2004) 259–269.
[8] C.T. Liu, J.O. Stiegler, Science 226 (1984) 636–642.
[9] R. Thomson, C. Hsieh, V. Rana, J. Appl. Phys. 42 (1971) 3154–3160.
[10] T. Zhu, J. Li, S. Yip, Proc. R. Soc. A 462 (2006) 1741–1761.
[11] S.L. Zhang, T. Zhu, T. Belytschko, Phys. Rev. B 76 (2007) 094114.
[12] G. Schoeck, W. Pichl, Phys. Status Solidi A 118 (1990) 109–115.
[13] J.C.H. Spence, Y.M. Huang, O. Sankey, Acta Metall. Mater. 41 (1993) 2815–2824.
[14] S. Kohlhoff, P. Gumbsch, H.F. Fischmei, Philos. Mag. A 64 (1991) 851–878.
[15] R. Pérez, P. Gumbsch, Phys. Rev. Lett. 84 (2000) 5347–5350.
[16] W.S. Walston, K.S. O'Hara, E.W. Ross, T.M. Pollock, W.H. Murphy, René N6: Third generation single crystal superalloy. Miner. Met. and Mater. Soc., Warrendale, PA, 1996, pp. 27–34.
[17] G.L. Erickson, The development and application of CMSX-10. Miner. Met. and Mater. Soc., Warrendale, PA, 1996, pp. 35–44.
[18] X.X. Yu, C.Y. Wang, Philos. Mag. 92 (2012) 4028–4039.
[19] Y.J. Wang, C.Y. Wang, Scripta Mater. 61 (2009) 197–200.
[20] X.X. Yu, C.Y. Wang, Mater. Sci. Eng., A 539 (2012) 38–41.
[21] S.L. Liu, C.Y. Wang, T. Yu, Z.G. Liu, Comput. Mater. Sci. 97 (2015) 102–108.
[22] X.Y. Yang, W.Y. Hu, J. Appl. Phys. 115 (2014) 153507.
[23] S. Wöllmer, T. Mack, U. Glatzel, Mater. Sci. Eng., A 319 (2001) 792–795.
[24] D.E. Ellis, G.A. Benesh, E. Byrom, Phys. Rev. B 16 (1977) 3308.
[25] D. Guenzburger, D.E. Ellis, Phys. Rev. B 45 (1992) 285.
[26] G.C. Sih, H. Liebowitz, Mathematical Theories of Brittle Fracture, Fracture: an Advanced Treatise, vol. II, Academic Press, New York, 1968. pp 69–189.
[27] M.P. Allen, D.J. Tildesley, Computer Simulation of Liquids, Oxford University Press, New York, 1987. p. 83.
[28] J.P. Du, C.Y. Wang, T. Yu, Model. Simul. Mater. Sci. Eng. 21 (2013) 015007.
[29] Q.N. Fan, C.Y. Wang, T. Yu, J.P. Du, Phys. B 456 (2015) 283–292.
[30] Z.G. Liu, C.Y. Wang, T. Yu, Comput. Mater. Sci. 83 (2014) 196–206.
[31] Z.G. Liu, C.Y. Wang, T. Yu, Model. Simul. Mater. Sci. Eng. 21 (2013) 045009.
[32] J. Rifkin, Center for Simulation, University of Connecticut, CT. <http://www.xmd.sourceforge.net/>.
[33] X.X. Yu, C.Y. Wang, X.N. Zhang, P. Yan, Z. Zhang, J. Alloy. Compd. 582 (2014) 299–304.
[34] Y. Zhou, Z.G. Mao, C.B. Morrison, D.N. Seidman, Appl. Phys. Lett. 93 (2008) 171905.
[35] Y. Amouyal, Z.G. Mao, D.N. Seidman, Acta Mater. 58 (2010) 5898–5911.
[36] D. Blavette, E. Cadel, C. Pareige, B. Deconihout, P. Caron, Microsc. Microanal. 13 (2007) 464–483.
[37] Y. Mishin, Acta Mater. 52 (2004) 1451–1467.
[38] R. Hill, Proc. Phys. Soc. London A 65 (1952) 349–354.
[39] G. Grimvall, Thermophysical Properties of Materials, North-Holland, Amsterdam, 1999.
[40] Y.J. Wang, C.Y. Wang, Philos. Mag. 89 (2009) 2935–2947.
[41] Y.J. Wang, C.Y. Wang, Mater. Res. Soc. Symp. Proc. 1224 (2010). FF05–31.
[42] D.E. Kim, S.L. Shang, Z.K. Liu, Intermetallics 18 (2010) 1163–1171.
[43] A.F. Voter, S.P. Chen, Mater. Res. Soc. Symp. Proc. 82 (1987) 175–180.
[44] P. Gumbsch, R.M. Cannon, MRS Bull. 25 (2000) 15–20.
[45] S.G. Lekhnitskii, Theory of an Anisotropic Body, Holden-Day, San Francisco, 1963. p. 109.
[46] P.A. Gordon, T. Neeraj, Acta Mater. 57 (2009) 3091–3100.
[47] C.Y. Wang, D.L. Zhao, Mater. Res. Soc. Symp. Proc. 318 (1994) 571.
[48] F.H. Wang, C.Y. Wang, Phys. Rev. B 57 (1998) 289.
[49] D.E. Ellis, G.S. Painter, Phys. Rev. B 2 (1970) 2887.
[50] D.E. Ellis, J. Guo, in: D.E. Ellis (Ed.), Electronic Density Functional Theory of Molecules, Clusters and Solids, Kluwer, Dordrecht, 1995, p. 263.